Multistep anchoring of a catalytically active ruthenium complex in porous mesostructured silica

Stéphanie Calmettes,[a] Belén Albela,[a] Olivier Hamelin,[b] Stéphane Ménage,[b] Fabien Miomandre[c] and Laurent Bonneviot*[a]

Received (in Montpellier, France) 6th November 2007, Accepted 14th January 2008
First published as an Advance Article on the web 11th February 2008
DOI: 10.1039/b717190k

A supported [Ru(dmp)$_2$(Py@LUS)Cl]Cl complex (dmp = 2,9-dimethyl-1,10-phenantroline) was synthesised in LUS, a 2D hexagonal porous mesostructured silica, *via* a step-by-step approach for the sake of site isolation, unicity and localisation in the confined space of the nanopores of the silica matrix. A pyridine terminated tether, Py@LUS, was homogeneously distributed on the surface using a molecular stencil patterning technique, followed by reaction of [Ru(dmp)$_2$Cl$_2$] at 78 °C. All intermediate materials were thoroughly characterised with a panel of techniques, including X-ray diffraction, elemental analysis, ^{29}Si and ^{13}C solid state NMR, diffuse reflectance UV-vis and FT-IR spectroscopies, and cyclovoltamperometry. Site isolation, unicity and localisation are achieved in the confined space of the nanopores of the silica matrix. The final material is selectively active in the catalytic oxidation of methylphenylsulfide into sulfoxide.

1. Introduction

Heterogenisation of metallic complexes has been extensively used in key catalytic reactions,[1] because the immobilisation of active sites on supports leads to better robustness and recyclability of the systems, compared to homogeneous ones. More interestingly, in some cases the fixation of the catalyst can also lead to an improvement of selectivity.[2] In fact, nature shows us that prearrangement of some functions near the active site of metalloproteins favours selectivity.[3,4] In this vein, Coman *et al.*[5] showed that when using mesoporous molecular sieves as support, stereoselectivity can be enhanced most likely due to a confinement effect in the pores of the structure.[6]

On an other hand, ruthenium complexes have been broadly used in catalytic reactions, such as hydrogenations, oxidations, C–C bond creations or reactions with CO and CO_2.[7,8] Among them, Ru(diimine) complexes (diimines such as 1,10-phenantroline or 2,2′-bipyridine) represent an important class of active catalyst for epoxidation, hydroxylation and sulfoxidation.[9] The prototype of this class, [Ru(bipy)$_2$(py)L] (where L is a monodentate labile ligand) has been fully studied in terms of reactivity, and mechanistic studies have demonstrated the involvement of [Ru(IV)=O(bipy)$_2$(py)] as the active species.[10] To our knowledge, there is not yet any report on the incorporation of such ruthenium complexes into the confined space of pores with a well-defined size. This prompts us to design a mesoporous phase containing covalently bound complexes. The complex [Ru(dmp)$_2$ (Py)Cl]$^+$ was chosen because of its high structural stability and its potential application in enantioselective catalysis.[11] There is a rich chemistry of complex fixation inside hexagonal or cubic mesostructured silica.[12,13] The silica's very well defined porous structure is an essential point in the approach of controlling each step of the synthesis and functionalisation of materials.[14,15] In our case, two main routes of synthesis of supported metal complex in mesoporous matrix may be applied: first the co-condensation of ligands[16,17] or metallic complexes[18,19] with the silica source in the sol–gel synthesis, and second the post-functionalisation[20] by reaction of the preformed mesostructured silica with moieties to be incorporated. For this last route, one may synthesize a catalyst by mere physical deposition[21] or by covalent grafting. The former allows to obtain a metal rich catalyst (usually >5 wt%), but with a rather low metal dispersion, limited in efficiency, robustness and recyclability for catalysis. The covalent route consists in anchoring a homogeneous catalyst onto a support by chemical tethering,[22,23] that avoids direct bonding to the silica surface and minimises the risk of structural modification of the complex. However, this approach does not allow full control of the metal coordination, which may still react with the remaining surface silanol groups and modify its properties.[24] In addition, direct grafting of the complexes in a confined space is a difficult task because of steric hindrance and diffusion restrictions.[25] The alternative is to develop a ship-in-the-bottle method that may appear long but could be worthy for application in the fine chemical industry.[26] It necessitates the control of the molecular design at each step of the synthesis implying organosilanes for tethering. These molecules usually contain on one part a ethoxy-, methoxy- or chlorosilane function and on the other part functional organic moities. The former is necessary for anchoring the tether *via* the reaction with the surface silanols by formation of siloxane "Si–O–Si" bridges. The latter is chosen to covalently bind a ligand to generate the targeted

[a] *Laboratoire de Chimie, Ecole normale supérieure de Lyon, Institut de Chimie Lyon, Université de Lyon, 46 allée d'Italie, 69364 Lyon cedex 7, France. E-mail: laurent.bonneviot@ens-lyon.fr; Fax: +33 (0)4 72 72 88 60; Tel: +33 (0)4 72 72 83 91*
[b] *Laboratoire de Chimie et Biologie des Métaux, UMR CEA-UJF-CNRS no 5249, IRTSV, CEA-Grenoble, 17 Avenue des martyrs, 38054 Grenoble Cedex 9, France*
[c] *Laboratoire de Photophysique et Photochimie Supramoléculaires Macromoléculaires, UMR CNRS 8531, Ecole normale supérieure de Cachan, 61 avenue du Président Wilson, 94230 Cachan, France*

coordination. There are very few reports on such stepwise design of complexes in confined space.[26]

In the present study, the step-by-step building of a tether terminated by a pyridyl moiety (Py@LUS) in mesostructured silica is proposed. The last step consists of the fixation of ruthenium by the reaction of the solid with $Ru(dmp)_2Cl_2$, which should lead to the formation of $[Ru(dmp)_2$-(Py@LUS)Cl][Cl], a grafted analogue of the targeted species. The mesostructured porous silica chosen here is the so-called LUS[27] (Laval University Silica) with a MCM-41 like structure. Its organic functionalisation is performed according to a specific technique developed by some of us.[28] The latter is briefly described here and is designed to combine an homogeneous dispersion of the tether with hydrophobisation of the surface, leading to a "molecular stencil patterning".[29] Finally, preliminary studies allow us to describe the obtained material as an efficient catalyst for the selective oxidation of sulfide into sulfoxide by H_2O_2.

2. Experimental

2.1 Materials

Low-angle X-ray powder diffraction experiments have been carried out with a Bruker (Siemens) D5005 diffractometer using Cu Kα monochromatic radiation. Nitrogen adsorption–desorption isotherms at 77 K were determined with a volume device Micromeritics ASAP 2010M. Infrared spectra were recorded from KBr pellets using a Mattson 3000 IRTF spectrometer. Liquid UV-vis spectra were recorded using a Vector 550 Bruker spectrometer. Solid UV-vis and near infrared spectra were recorded from aluminium cells with Suprasil 300 quartz windows, using a PerkinElmer Lambda 950 and PE Winlab software. ^{13}C and ^{29}Si solid NMR measurements were collected on a Bruker DSXv400 spectrometer. For ^{13}C (100.6 MHz) CPMAS solid NMR, a 5 μs ($\theta = \pi/2$) pulse was used with a repetition of 4 s; the spinning rate of the rotor was about 5 kHz and the number of scans was situated between 2000 and 15 000. For ^{29}Si (79.49 MHz) MAS solid NMR, a 5 μs ($\theta = \pi/2$) pulse was used with a repetition time of 80 s; the spinning rate of the rotor was about 10 kHz and the number of scans 512. TGA measurements were collected from Al_2O_3 crucibles on a DTA-TG Netzsch STA 409 PC/PG instrument, under air (30 mL min^{-1}), with a 25–1000 °C (10 °C min^{-1}) temperature increase. GC-MS analysis was done with a Perkin-Elmer autosystem X coupled to a turbomass spectrometer.

2.2 Syntheses

As-made silica 1. LUS mesoporous silica with hexagonal structure was synthesized following a described procedure:[28] NaOH (32.0 g) was solvated in deionised water (800 mL), and then a colloidal solution of silica (187 mL) (Ludox, HS-40 colloidal silica, 40 wt% suspension in water) (Sigma-Aldrich) was added. Precipitation happened immediately when the mixture was formed but a nearly clear solution of sodium silicate was formed after stirring the mixture at 40 °C for 24 h. A solution of hexadecyltrimethylammonium-*p*-toluene-sulfonate CTATos (12.8 g) (>99%, Merck) in deionised water (462 mL) was stirred for 1 h at 60 °C. 320 mL of the Na_2SiO_3 solution were stirred for 1 h at 60 °C too, and then added dropwise into the CTATos solution. The mixture was stirred for 2 h at 60 °C and then loaded into four 250 mL Teflon-lined steel autoclaves where it was statically heated for 20 h at 130 °C. The resulting white precipitate was filtered, washed with deionised water (3 × 50 mL), and dried at 80 °C for one night, leading to 12 g of as-made LUS **1**. Anal. found (%): C 32.7, H 6.9, N 2.0, S 0.4, weight loss at 1000 °C, 50.7%.

Partially extracted silica 2. As-made material **1** (6 g) was solvated in technical ethanol (250 mL) and stirred at 40 °C for a few minutes, then diluted hydrochloric acid (4.25 mL, 0.5 eq) (1 mol L^{-1}, standard) (Acros) was added. The mixture was stirred at 40 °C for 1 h, then filtered, washed with technical ethanol (2 × 50 mL), technical acetone (2 × 50 mL), and dried at 80 °C for one night, leading to 4 g of partially extracted silica **2**. Anal. found (%): C 20.0, H 4.6, N 1.1, S < 0.3, weight loss at 1000 °C, 34.4%.

Partially silylated silica 3. Material **2** (4 g) was placed in a round bottom two-neck flask where it was dried at 150 °C under argon flow for 1 h, then under vacuum for 2 h. After being brought back to room temperature, cyclohexane (100 mL) (synthesis grade, SDS) and hexamethyldisilazane HMDSA (18 mL, 30 eq.) (98%, Alfa Aesar) were added to the flask, and the mixture was stirred at room temperature for 1 h, and refluxed for 18 h. The mixture was filtered, washed with cyclohexane (2 × 20 mL), technical ethanol (2 × 20 mL), technical acetone (20 mL), and dried at 80 °C for one night. All these steps were repeated two more times, leading to 4 g of partially silylated silica **3**. Anal. found (%): C 20.2, H 4.3, N 0.8, S < 0.3, weight loss at 1000 °C, 25.0%.

Extracted silica 4. Material **3** (4 g) was solvated in technical ethanol (250 mL) and stirred at 0 °C for a few minutes, then diluted hydrochloric acid (4.5 mL, 1.1 eq, 1 mol L^{-1}) was added. The mixture was stirred at 0 °C for 1 hour, then filtered, washed with technical ethanol (2 × 50 mL), technical acetone (2 × 50 mL), and dried at 80 °C for one night, leading to 3 g of extracted silica **4**. Anal. found (%): C 8.0, H 2.4, N < 0.1, S < 0.3, weight loss at 1000 °C, 10.5%.

Functionalised silica 5. Material **4** (1 g) was placed in a round bottom two-neck flask where it was dried at 130 °C under argon flow for 1 h, then under vacuum for 2 h. Back at room temperature, 15 mL of distilled toluene (synthesis grade, SDS) and 1 mL (5 eq.) of isocyanatopropyl-dimethylchlorosilane (95%, ABCR) were added to the flask, then the mixture was stirred at room temperature for 1 h, and refluxed for 20 h. The obtained product was washed with distilled toluene (10 mL three times) under argon, then directly solvated in 15 mL of freshly distilled dichloromethane (synthesis grade, SDS). Then 0.5 mL (3 eq) of 4-aminomethylpyridine (98%, Aldrich) was added dropwise. The mixture was stirred at room temperature under argon for 24 h, then filtered, washed with dichloromethane (2 × 30 mL) and technical acetone (2 × 30 mL), and dried under vacuum at room temperature. The obtained product was then re-solvated in 75 mL of ethanol (analytical grade, VWR) at 0 °C. The mixture was stirred for 1 h, then washed with ethanol (2 × 30 mL) and acetone

(2 × 30 mL) (analytical grade, VWR), and dried under vacuum at room temperature, leading to 0.7 g of functionalised silica **5**. Anal. found (%): C 13.6, H 3.0, N 1.7, S < 0.3 , weight loss at 1000 °C, 17.1%.

Ruthenium supported complex 6. Material **5** (200 mg) was solvated in 30 mL of ethanol under argon, at room temperature. Then 106.6 mg (1 eq.) of ruthenium complex $Ru(dmp)_2Cl_2$ (dmp = (2,9)-dimethyl-1,10-phenantroline) was added, and the mixture was stirred during 3 h at 78 °C, under argon and protected against light. The obtained solid was washed with ethanol (10 mL, several times) until filtrates became colourless, leading to 230 mg of ruthenium supported complex **6**. Anal. found (%): Ru 1.1, Cl 1.1, C 11.9, H 2.4, N 1.6, S < 0.3, weight loss at 1000 °C, 20.9.

2.3 General procedures

Electrochemical measurements. Cyclic voltammetry of ruthenium precursors (**[Ru1]** = $Ru(dmp)_2Cl_2$ and **[Ru2]** = $[Ru(dmp)_2PyCl][PF_6]$) was performed with a CH Instruments 600B potentiostat in a three-electrode cell. A platinum disk (1 mm diameter) was used as the working electrode, a platinum wire as the auxiliary electrode, and an $AgNO_3|Ag$ electrode as the reference. This latter was checked *vs*. ferrocene as recommended by IUPAC (E°_{Fc} = 0.100 V). The electrolyte was a solution of tetrabutylammonium hexafluorophosphate (TBAP, 0.1 M) in CH_2Cl_2, and the scan rate was 50 mV s^{-1}.

The electrochemical response of supported ruthenium solids was analyzed by means of a home-built potentiostat equipped with an efficient ohmic drop compensation, in a three-electrode cell, using slow and fast scan rate cyclic voltammetry. This study was performed in CH_2Cl_2 with TBAP (Fluka, puriss.) 0.1 M as the supporting electrolyte. The solid was coated on the working electrode by drying a solution containing 5% polystyrene (Aldrich, average molar mass: 280 000) mixed with the functionalised silica powder (20 mg) in dichloromethane. Solutions were deaerated by argon bubbling for 10 min prior to each sequence of measurements.

Catalytic sulfoxidation. 21 μL of methylphenylsulfide (600 eq) were added to an acetone solution of catalyst material **6** (0.3 mM), and the reaction was initiated by addition of 0.43 μL (15 eq) of H_2O_2 (35% in water). The reaction was monitored by gas chromatography from the amount of methylphenylsulfoxide formed using benzophenone (5 μL of a 1 M solution in dichloromethane) as internal standard.

3. Results

Supported ruthenium complex **6** is synthesised according to the following step-wise sequence (Scheme 1). The first four steps deal with the preparation of the surface by the so-called molecular stencil patterning,[29] the fifth step combines two reactions to built up the pyridyl tether Py@LUS, and the last one consists in the metallation of the solid *via* complexation of the ruthenium complex with Py@LUS. In Scheme 1, the internal surface of the channel is represented as a flat surface for the sake of simplification. First as-made LUS **1** is obtained following a described procedure,[28] then a controlled addition of hydrochloric acid leads to material **2**, in which the remaining surfactant is supposed to be homogeneously dispersed, because of the electronic repulsion between the cationic heads of these molecules. Then material **3** is obtained *via* reaction of hexamethyldisilazane (HMDSA) with surface silanol available between the remaining surfactant (CTA^+), playing the role of stencil. The self repulsion between these cationic molecules creates the patterning effect.[29] In the next step, the remaining surfactant is extracted using an addition of hydrochloric acid (1.1 eq) at 0 °C. These specific conditions were found the be imperative to insure an effective removal of the surfactant without removal of the TMS surface groups in material **4**. Then, molecules of isocyanatopropyldimethyl chlorosilane are grafted, and directly engaged with 4-aminomethylpyridine because of the high reactivity of the isocyanate group. The linkage of the pyridine moieties Py@LUS is obtained by the formation of a urea function in material **5**. Then $Ru(dmp)_2Cl_2$ is used as ruthenium precursor, and is introduced in the solid to react with the Py@LUS tether in mild conditions. The material **6** so obtained (after thorough washing) has a dark purple color.

X-Ray diffraction patterns of the obtained materials reveal that the hexagonal structure of the materials is maintained through all the sequence of synthesis, from as-made LUS **1** to the supported ruthenium complex in material **6** (Fig. 1). Furthermore, for materials **1–6**, cell parameter and half-width at half-height (HWHH) remain quite similar, which shows that the pore size and distribution do not change during the sequence of treatments undergone by the solids (Table 1). The intensity of the peak 100 is consistent with the evolution of the materials: it first increases when the surfactant is partially removed during the synthesis of material **2**, then it remains constant for materials **3** to **5**, for which modifications are made at the surface, and finally decreases upon the introduction of the ruthenium complex.

The low temperature nitrogen adsorption–desorption isotherms of material **6** and the parent material **1** are similar and classified as type (IV) according to the IUPAC nomenclature.[29] This is also characteristic of mesostructured porous material.[30] The obtained profiles account for a narrow pore size distribution and a small average size diameter decreasing from 3.0 in material **1** to 2.5 in material **6** according to the BJH model (Table 1). This decrease is consistent with a partial filling of the pores by the ruthenium complex. The surface after grafting of the complex is concomitantly reduced from 1030 to 615 m^2 g^{-1}.

The different steps of functionalisation of the surface in the solids **1** to **6** were followed with several techniques, such as elemental analysis and thermogravimetric measures (TGA), ^{13}C and ^{29}Si NMR, IR and solid UV-vis spectroscopies, and electrochemistry.

First, elemental analysis (Table 2 and 3) shows that as-made LUS **1** contains 0.17 mol of surfactant per mol of inorganic silica, which corresponds to 74% of the covered surface, assuming that 0.23 mol of grafted function per mol of inorganic SiO_2 corresponds to 100% coverage.[28,31] This value is directly derived from the molar ratio N : SiO_2. After partial extraction with acid treatment, material **2** still contains 0.07 mol of surfactant standing for a removal of 41% of the surfactant, and corresponding to *ca*. 30% coverage.

In eqn (1) (see below), the molar ratios N/SiO_2 and C/SiO_2 (Table 2) are denoted *N* and *C*, respectively. It designs the

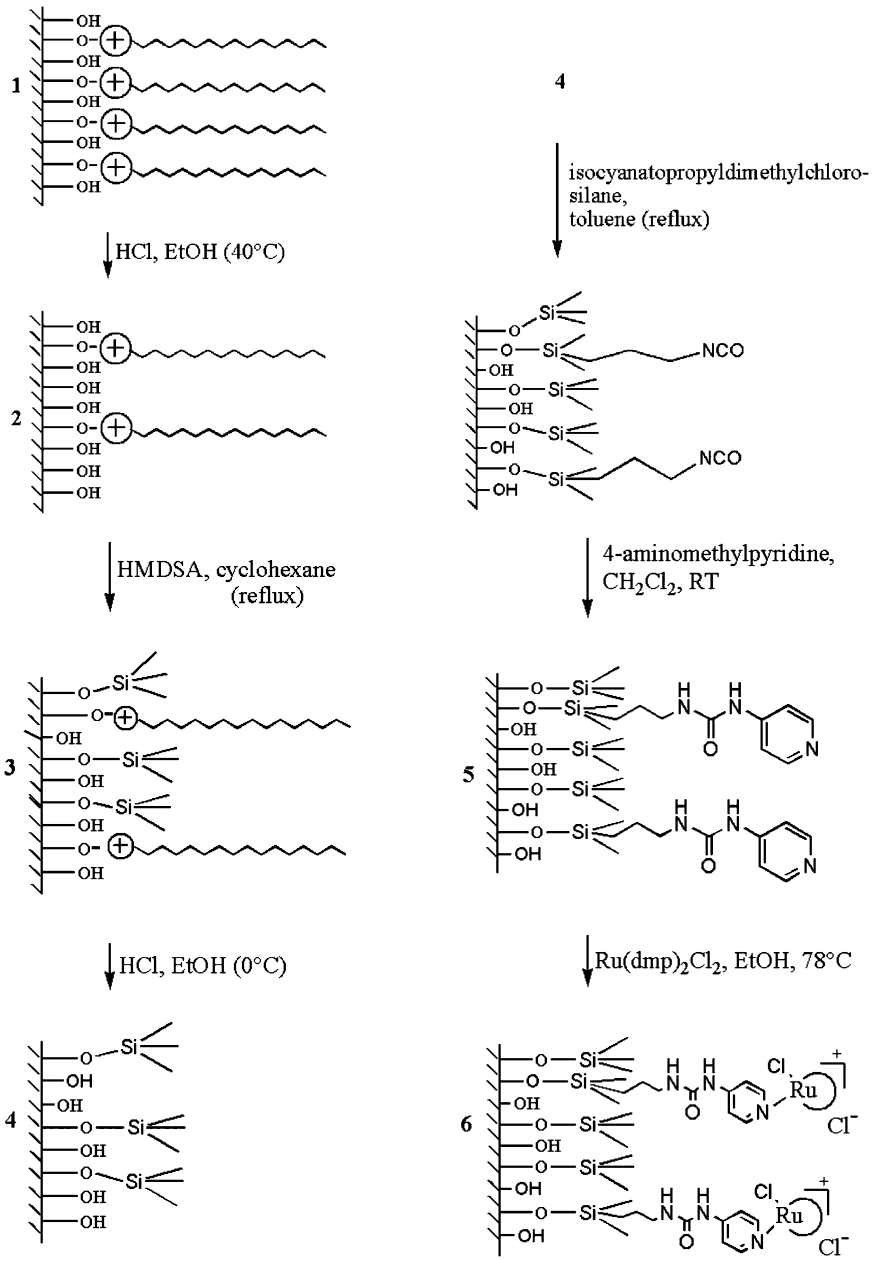

Scheme 1 Step-by-step functionalisation from as-made silica LUS **1** to ruthenium supported complex **6**.

global amount of nitrogen and carbon atoms that are present in a material. Considering that carbon atoms account for both surfactant ($C_{19}NH_{42}$) and TMS (C_3SiH_9) species, the molar amount of TMS (n_{TMS}) is deduced as follows:

$$n_{TMS} = \frac{C - 19 \times N}{3} \quad (1)$$

According to eqn (1), the surface of material **3** is covered at 87% by TMS, distributed among the remaining surfactant. In material **4**, it is assumed that there is no surfactant left in the channels in order to calculate the other figures. Thus for material **5**, the nitrogen atoms come from tether molecules only. According to TGA measurements, the distribution of urea tethers has been estimated as 3 : 1 ($C_{12}N_3H_{20}OSi$–Py@-LUS : $C_{11}N_2H_{26}OSi_2$–urea **9**). These formulas correspond to two possible forms of grafted molecules (see discussion and Scheme 2). The system is also assumed to contain *ca.* 15% of free aminomethylpyridine ($C_6N_2H_7$). So the amount of urea tethers (n_{urea}) and the amount of TMS (n_{TMS}) are deduced from the following equations:

$$n_{urea\,\mathbf{9}} = \frac{n_{urea\,\mathbf{5}}}{3} \quad (2.1)$$

$$n_{free\ pyridine} = 0.15\,(n_{urea\,\mathbf{5}} + n_{urea\,\mathbf{9}}) = 0.2\,n_{urea\,\mathbf{5}} \quad (2.2)$$

$$n_{urea\,\mathbf{5}} = \frac{N}{4.06} \quad (2.3)$$

$$n_{TMS} = \frac{C - (12n_{urea\,\mathbf{5}} + 11n_{urea\,\mathbf{9}} + 6n_{free\ pyridine})}{3} \quad (2.4)$$

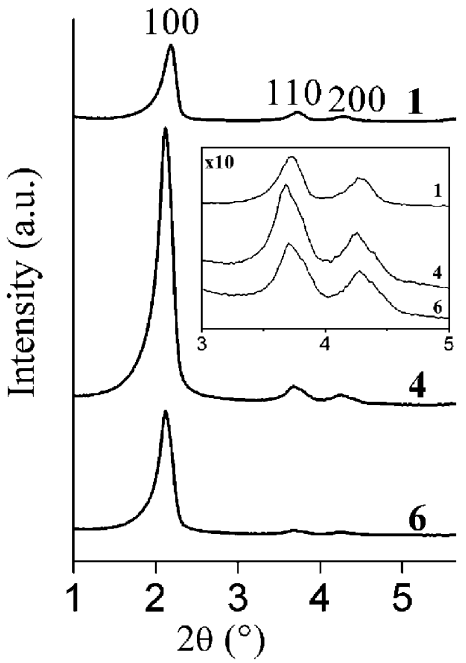

Fig. 1 X-Ray powder diffraction pattern for materials **1** (as-made LUS), **4** (extracted silica) and **6** (ruthenium supported complex). Insert: enlarged region for 110 and 200 peaks (×10).

Table 1 Textural properties of materials **1–6**

Material	**1**	**2**	**3**	**4**	**5**	**6**
d_{100}/nm	4.1	4.0	4.1	4.1	4.1	4.2
a_0[a]/nm	4.7	4.6	4.7	4.7	4.7	4.8
Intensity[b]/10^3 counts	30	80	110	110	120	50
HWHH[c] 2θ/°	0.22	0.26	0.22	0.22	0.22	0.20
BET surface area/m^2 g^{-1}	1030	—	—	—	—	615
Porous volume/mL g^{-1}	0.96	—	—	—	—	0.46
Pore diameter[d]/nm	3.0	—	—	—	—	2.5

[a] Parameter calculated from d_{100} with the formula $a_0 = 2*d_{100}/3^{1/2}$. [b] Height at the maximum of (100) peak. [c] Half-width at half-height. [d] Using BJH method.

Table 2 Elemental analysis for materials **1–6**

Material	**1**	**2**	**3**	**4**	**5**	**6**
C/SiO_2[a]	3.32	1.52	1.62	0.53[b]	1.04	0.98
N/SiO_2[a]	0.17	0.07	0.05	<0.01[c]	0.11	0.11
Cl/SiO_2[a]	—	—	—	—	—	0.02
Ru/SiO_2[a]	—	—	—	—	—	0.008

[a] Molar ratio calculated considering inorganic SiO_2 content obtained from weight loss at 1273 K and removing the contribution of the organic SiO_2 formed from the grafted silane. [b] After extraction, *n*(surfactant) is assumed to be zero (see) to estimate organic SiO_2. [c] Maximal value due to the detection limit of elemental analyser (0.1% in nitrogen).

These equations lead to surface coverages of *ca.* 78 and 18% for TMS and urea tethers, respectively. At last, in material **6** the molar ratio Ru/SiO_2 allows the evaluation of the number of carbon and nitrogen atoms that were brought into the system by the complex ($RuC_{28}N_4H_{24}$). After removing this contribution, carbon and nitrogen atom ratios have been found to be lower than the former ones in material **5**. The extraction of free aminomethylpyridine molecules is not sufficient to explain this decrease. Nevertheless, no loss of urea functions has been observed by IR spectroscopy. This suggests a loss of TMS or a rearrangement of grafted ureas during the introduction of ruthenium complex.

In the following, ^{29}Si MAS NMR (Fig. 2) and IR spectra (Fig. 3 and 4) are described in terms of the quantitative evolution of various surface species, starting from step **3** to the end. The ^{29}Si MAS NMR spectra exhibit a signal at 15 ppm, assigned to M type silicon (**Si**C_3O), corresponding to grafted TMS and/or urea tether groups. Unfortunately both signals are superimposed and cannot be differentiated. A group of signals, mainly composed of Q_3 (**Si**$(OH)O_3$, ~−100 ppm) and Q_4 (**Si**O_4, ~−110 ppm) species is also observed between −90 and −110 ppm. The latter are usually assigned to silanol and bulk silicon of the matrix silica.[32] The Q signals accounted for as inorganic silicon (Si_{inorg}), while the M type is related to organic silicon (Si_{org}), as defined in Table 2. Thus, Si(M)/Si(Q) ratios of 0.14 and 0.13 for materials **3** and **4**, respectively, show that the TMS groups remain grafted on the surface during the extraction of the surfactant. In the next step, this ratio reached the value of *ca.* 0.22, consistent with the completion of the surface coverage by the grafted isocyanate tethers and their reaction with 4-aminomethylpyridine (remember that 0.23 corresponds to 100% coverage, as explained above).

For IR spectroscopy, the window 650–1000 cm^{-1} (Fig. 3) allows us to focus on the Si–C stretching vibrations (860 and

Table 3 Percentage of covered surface[a] for materials **1–6**

Material	**1**	**2**	**3**	**4**	**5**	**6**
Surfactant	74 ± 1 (0.17)[b]	30 ± 1 (0.07)	20 ± 1 (0.05)[b]	0[d]	0	0
TMS	—	—	87 ± 3 (0.20)[c]	77 ± 3 (0.17)	78 ± 3 (0.18)[e]	77 ± 3 (0.17)[f]
Molecular tethers	—	—	—	—	18 ± 3 (0.04)[e]	23 ± 3 (0.05)[f]

[a] Brackets: molar ratio of grafted function per mol of inorganic SiO_2. Assuming that 0.23 mol of grafted function per mol of inorganic SiO_2 corresponds to 100% coverage.[31] [b] In mole per mole of inorganic SiO_2. The amount of surfactant ($C_{19}NH_{42}$) is directly given by the molar ratio of nitrogen: *n*(surfactant) = N/SiO_2. [c] In mole per mole of inorganic SiO_2. The amount of trimethylsilyl (C_3H_9Si) is calculated by removing the contribution of the carbons of surfactant molecules to the total **5**. [d] After extraction, *n*(surfactant) assumed to be zero to estimate organic SiO_2. [e] In mole per mole of inorganic SiO_2. Tethers are assumed to be distributed 3 : 1 ($C_{12}N_3H_{20}OSi : C_{11}N_2H_{26}OSi_2$), see discussion. The amount of trimethylsilyl (C_3H_9Si) is calculated by removing the contribution of the carbons of tethers molecules to the total molar ratio of carbon, and by dividing this quantity by three. Here organic SiO_2 = Si (TMS) + Si (tethers). [f] Assuming that the amounts of trimethylsilyl and grafted tethers are the same in material **6** as in material **5**.

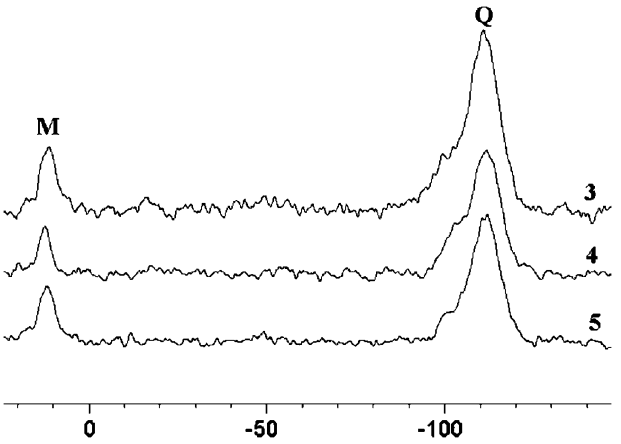

Fig. 2 ^{29}Si MAS NMR spectra for partially silylated silica (**3**), extracted silica (**4**) and functionalised silica (**5**); Si(M)/Si(Q) = 0.14, 0.13 and 0.22 for materials **3**, **4** and **5**, respectively.

780 cm^{-1}), and the Si–OH stretching vibration in silanols (960 cm^{-1}). In materials **3** and **4**, the intensity of ν(Si–C) appears quite similar, whereas the intensity of the peak at 980 cm^{-1} assigned to ν(Si–O$^-$) decreases, giving rise to a well defined peak at 960 cm^{-1} assigned to ν(Si–OH). This is consistent with the neutralisation of silanolate and the removal of the surfactant as depicted in Scheme 1. In material **5**, the peak assigned to ν(Si–C) increases while the peak of the ν(Si–OH) mode decreases upon the grafting of urea tethers. For material **6**, the intensity of ν(Si–OH) seems to be slightly higher. Unfortunately, the IR spectrum of the ruthenium precursor Ru(dmp)$_2$Cl$_2$ exhibits Csp^2–H aromatic bending vibrations at 860 and 850 cm^{-1}, which prevents us being fully conclusive about the level of the silylation process in this material.

The introduction of the tether and the complex led to profound spectroscopic changes. The overall IR spectrum (Fig. 4) obtained for material **5** exhibits large bands with maxima at 1660 cm^{-1} and 1570 cm^{-1}, which are likely to be attributed to C=O stretching and N–H bending, respectively, typical urea functions.[33] In addition, ^{13}C CPMAS NMR spectra exhibit signals at $\sim$−5, 12, 20 and 45 ppm that are assigned to C_1, C_2, C_3 and C_4 carbon atoms, respectively, and are related to the isocyanate tether (Fig. 5). Signals are also observed at $\sim$120, 140 and 156 ppm, which correspond to the aromatic carbons of the pyridinyl group (C8 and C7,9) and to the carbon of the urea function (C5), respectively.

The former signals show that the isocyanate tether was grafted, and the latter signals are a fingerprint of the coupling reaction between the isocyanate previously grafted and the amino group of 4-aminomethylpyridine, leading to the global tether Py@LUS. Efficient washing was achieved with ethanol in order to remove unreacted 4-aminomethylpyridine. Finally, the ^{13}C NMR spectrum of material **6** exhibits multiple peaks, whose attribution was found to be difficult (data not shown). Nevertheless, the great changes observed between the NMR spectra for material **5** and that for material **6** directly illustrate the introduction of the ruthenium complex onto the solid.

The solid diffuse reflectance UV-vis spectra of materials **5**, **6** and references **[Ru1]** = Ru(dmp)$_2$Cl$_2$ and **[Ru2]** = [Ru(dmp)$_2$-PyCl][PF$_6$] were treated using the Kulbeka Munk function. They exhibit large bands (Fig. 6), consistent with the electronic transitions in solid state. The spectra of Ru^{II} containing samples feature intense intraligand $\pi \rightarrow \pi^*$ absorptions in the UV region, together with intense and broad d(Ru^{II}) $\rightarrow$ π^*(L) (L = dmp or grafted pyridine ligand) MLCT bands in the visible region. The UV-vis spectrum of material **5** exhibits only one maximum at $\sim$250 nm, characteristic of the anchored pyridine Py@LUS. For material **6**, the $\pi \rightarrow \pi^*$ absorptions appear as a large band at $\sim$274 nm with a shoulder at 295 nm, consistent with transitions of both the dmp ligand and the coordinated pyridine, respectively (*vide infra*). The MLCT bands present maxima at $\sim$390 and 500 nm for material **6**, slightly blue shifted compared to the ones of **[Ru1]** and **[Ru2]**. Both spectra of **[Ru1]** and **[Ru2]** appear similar, with $\pi \rightarrow \pi^*$ absorptions at $\sim$270 nm and MLCT bands with a single maximum at $\sim$500 nm. The similarity of the spectra obtained for material **6** and for **[Ru1]** and **[Ru2]** strongly suggest that the complex has been incorporated into the pores without degradation. Nevertheless, this

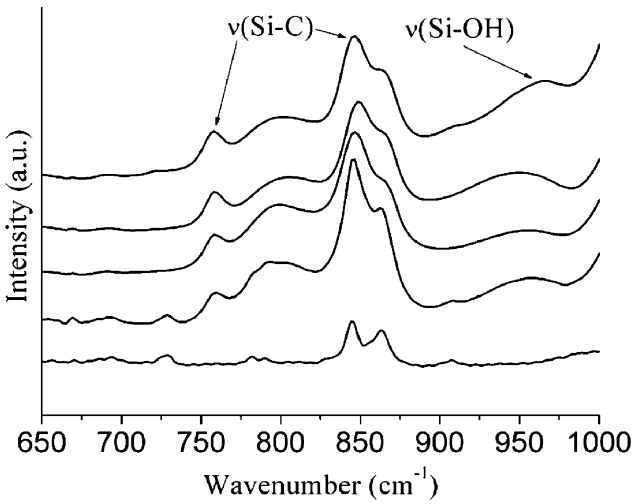

Fig. 3 Infra-red spectra of materials **3**, **4**, **5**, **6**, and ruthenium precursor **[Ru1]** = Ru(dmp)$_2$Cl$_2$, in the window 650–1000 cm^{-1}.

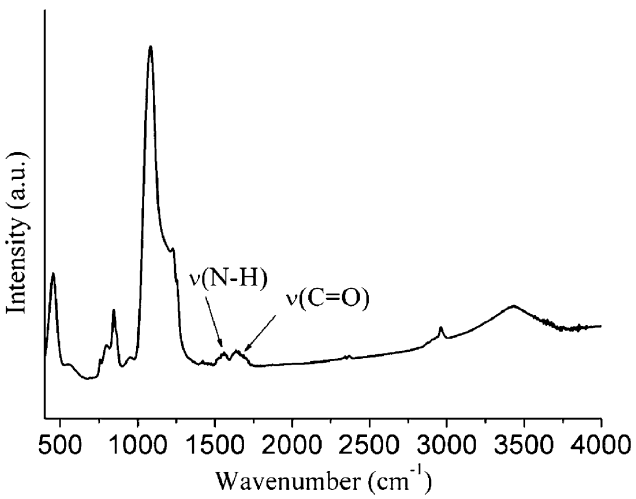

Fig. 4 Infra-red spectrum of material **5**.

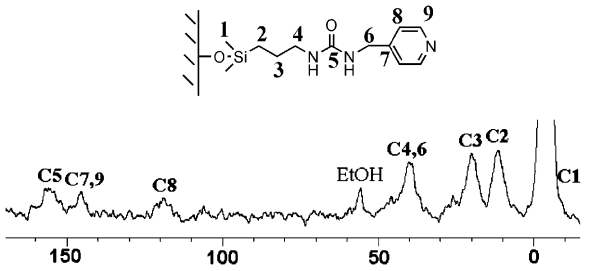

Fig. 5 ^{13}C CP-MAS NMR spectra of material **5** (functionalised silica).

technique can not be exploited to form a conclusion about the introduction of pyridine into the coordination sphere of the ruthenium.

The cyclic voltammograms of the reference compounds **[Ru1]** and **[Ru2]** show a reversible redox peak at $E^{\circ}_{ox} = -60$ mV *vs.* $AgNO_3|Ag$ for **[Ru1]**, and $E^{\circ}_{ox} = 550$ mV *vs.* $AgNO_3|Ag$ for **[Ru2]**, respectively. These peaks can be related to the oxidation $Ru^{II} \rightarrow Ru^{III}$ in both compounds, with the usual shift observed for a substitution of a chloride by a pyridine ligand, as reported in the literature.[34]

The response in cyclic voltammetry of the ruthenium grafted moieties in material **6** is shown Fig. 7 at various scan rates. The signal exhibits a pair of peaks emerging from a capacitive background current, corresponding to a single redox species with an oxidation standard potential of 500 mV *vs.* $Ag-NO_3|Ag$. In comparison with the values obtained for references **[Ru1]** and **[Ru2]**, this oxidation potential is consistent with a single type of ruthenium moiety in material **6** that has the expected chemical environment, *i.e.* one pyridine and one chloride ligand in the coordination sphere of Ru. The absence of remaining $Ru(dmp)_2Cl_2$ in the porous material **6** can be noted too.

Then, a very interesting feature is the evolution of log–log diagram of the oxidation current peak *versus* scan rate (Fig. 8). A linear relationship (slope of $\alpha = 0.64 \pm 0.02$) is obtained over three decades, showing that there is no transition in the mass transfer regime on the explored timescale. According to Laviron[35] and Andrieux *et al.*,[36] an electron hopping mechanism between homogeneously distributed redox sites in an isotropic medium should generate a variation of the peak current with the square root of the scan rate, since hopping can be assigned to a diffusion process.

Here, the electronic diffusion cannot be considered as isotropic, probably because of the 2D geometry of the channels in the mesostructured LUS. Similar current behaviour have been recently obtained in other materials, such as meso-structured porous nanocrystalline titanium oxide films.[36] Furthermore, the authors estimate that the Randles–Sevcik equation can be used to calculate the apparent diffusion coefficient, despite the non-classical diffusion mode observed here. This equation can be written:

$$D = \left(\frac{\beta}{0.44nFAC_{Ru}}\right)^2 \frac{RT}{nF} \qquad (3)$$

where n is the number of electrons exchanged per ruthenium species, A the electroactive area of the electrode, C_{Ru} the bulk

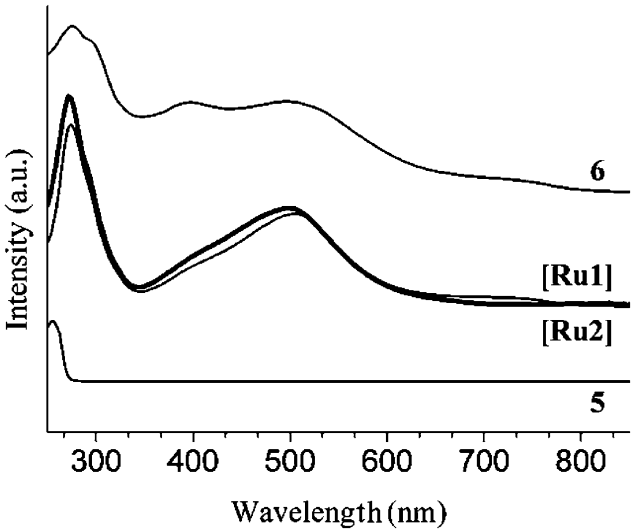

Fig. 6 Diffuse reflectance UV-vis spectra of material **5**, molecular references $[Ru(dmp)_2Cl_2]$ (**Ru1**, sharp line) and $[Ru(dmp)_2PyCl][PF_6]$ (**Ru2**, thick line) and material **6**.

concentration of Ru in the material and β is the slope of the I *vs.* $V^{1/2}$ relationship. In our case, one electron is exchanged, A was taken as the geometrical electrode area and C_{Ru} of *ca.* 10^{-4} mol cm^{-3} was calculated from the metal loading (1 wt% Ru) and the density (1.0) of the solid. These values lead to a diffusion coefficient of about 10^{-11} cm^2 s^{-1}. This order of magnitude is compatible with a diffusion process involving electron hopping between grafted electroactive species. This value is, however, notably smaller than in the case of mesoporous titania functionalised by ferrocene moieties,[37] probably because all the electroactive sites are not accessible in the case of the present material.

Finally, the catalytic activity of the supported complex **6** (0.3 mM) was assayed during oxidation of methylphenylsulfide (54 mM, 600 eq.) by hydrogen peroxide (4.5 mM, 15 eq.) in acetone. Evolution of the reaction was monitored by GC analysis using benzophenone as an internal reference. After 3 h

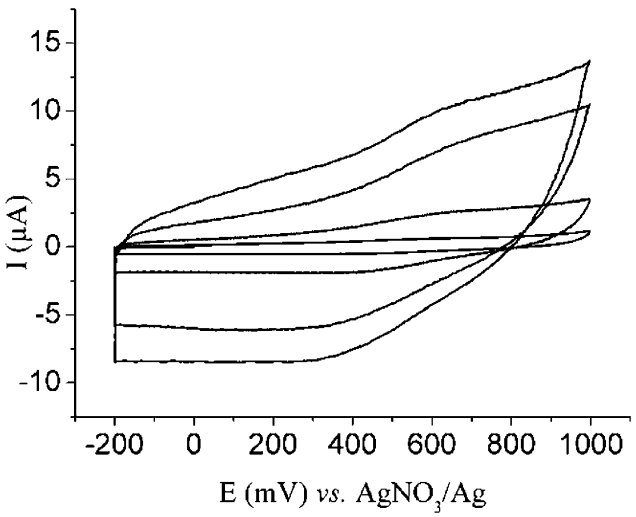

Fig. 7 Cyclic voltammograms of the ruthenium grafted material **6**, at the following scan rates (in V s^{-1}): (a) 0.2; (b) 1; (c) 5; (d) 10.

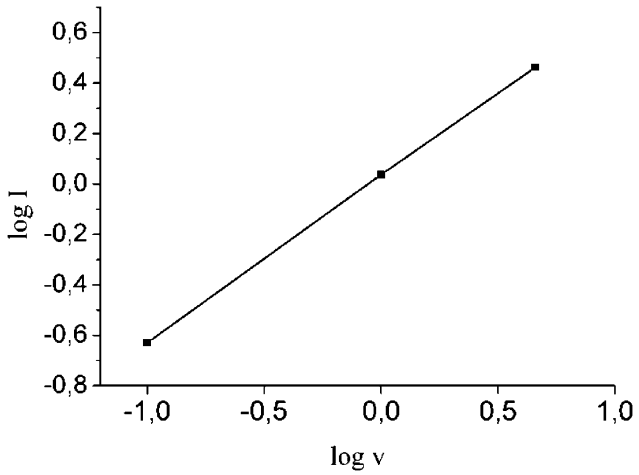

Fig. 8 Characteristic diagram of the cyclic voltammograms of Fig. 6; I/μA intensity of the oxidation peak current and V/mV s^{-1} scanning rate.

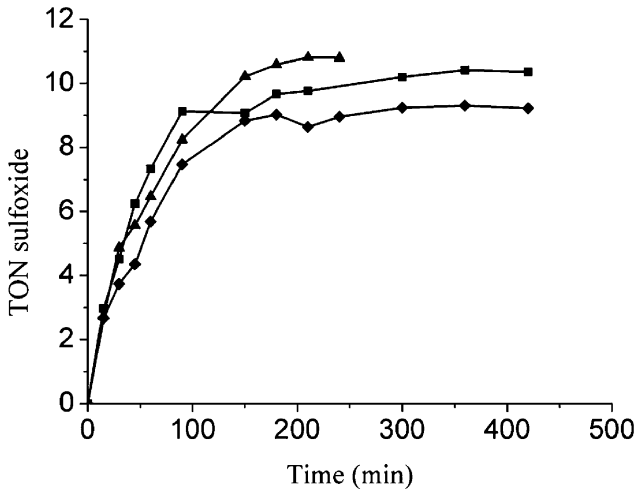

Fig. 9 Methylphenylsulfoxide TON showing the catalytic activity of material **6** for three successive cycles (**1**—◆, **2**—■ and **3**—▲).

of reaction at room temperature, the sulfide substrate reached a maximal yield in methylphenylsulfoxide of 73% (turn over number, TON, of 11) for material **6**.

Sulfone was also produced. Nevertheless, there was a high selectivity in sulfoxide (9 : 1 sulfoxide–sulfone). For comparison, the homogeneous catalyst [Ru(dmp)$_2$(4-methylpyridine)-Cl] [PF_6] was found to be active under these conditions (44% yield after 3 h, 7 TON). Blank experiments without catalyst or with material **5** were achieved and afforded 4% and 11% yield after 3 h, respectively. After filtration and washing with acetone, the recovered catalyst was engaged again in a second and a third run. Similar yields, selectivity and kinetics were observed (Fig. 9), consistent with a high stability of the catalyst in the material. Filtrates did not show any activity, which centred the reactivity on the heterogeneous species.

4. Discussion

The results show from various techniques of characterisation including UV-vis spectroscopy and voltamperometry, that the sequential synthesis approach adopted here leads to single ruthenium (II) sites anchored inside the channel of a 2D hexagonal silica. X-Ray diffraction patterns of the materials revealed indeed that the hexagonal structure of the materials was maintained all through the sequence of reactions involved. In addition, the supported complex **6** showed a good catalytic reactivity in the oxidation of methylphenylsulfide by H_2O_2, a high selectivity in sulfoxide and no apparent deactivation after three cycles of the reaction. Nevertheless, the aim of driving a quasi "molecular" approach of the sequential synthesis needs to be discussed particularly when considering the control of the nature and the quantity of grafted moieties at each step of the synthesis. These various points are treated in the following.

To obtain the best molecular stencil effect the TMS should not react or move during the acid extraction of the surfactant, to ensure site isolation, this is also needed to minimize in the following step the reaction of the isocyanate function with the surface silanol groups. The only information that may attest for such a problem relies on both the coverage level of TMS and type of linkage. For the latter, solid state ^{29}Si NMR exhibits very similar profiles at stage 3 and 4, anyhow, there is no indication in the literature that may differentiate the grafting of TMS on different types of silanol.[19,31] In addition, despite several trial the spectra were slightly different and found hardly exploitable for quantitative purpose. So a special effort was devoted to check this point using IR spectroscopy in the window 650–1000 cm^{-1} (Fig. 3) where Si–C stretching vibrations (780 and 860 cm^{-1}) specific to TMS were found free from any interference with other vibrational modes in materials **3** and **4**. All the spectra were calibrated using the deformation mode of SiO_2 at 450 cm^{-1} (not represented here but applied for spectrum of Fig. 3). Then, the intensity of the largest band at 860 cm^{-1} was chosen to monitor the TMS loading. No apparent change of intensity indicates a very similar coverage level. Actually, maintaining the TMS coverage during step (**3** → **4**) was found quite delicate and had necessitated a fine optimisation. Several experimental conditions were tested, changing the repetition time, solvent, temperature and quantity of HCl during this step. The data reported in terms of remaining TMS percentage (Fig. 10) shows that TMS anchoring was more fragile than expected. Both acetonitrile and ethanol were found similar with a drastic removal of about half of TMS at 40 °C only. Continuing with the less ethanol and decreasing the excess of hydrochloride acid from 10 to 1.1 eq (*vs.* surfactant) still led to a notable removal of *ca.* 20% even for a single washing. The best treatment that was finally adopted was 1.1 eq. of HCl, 1 time, at 0 °C. This shows that during displacement of the surfactant by neutralisation of the silanolate function, siloxane bridges that retained the TMS moieties may be hydrolysed most likely with acid catalytic assistance. Further studies about this specific problem are in progress to reach a better molecular control at this stage.

The quantification of the coverage was more delicate at the step **4** → **5** since the IR fingerprint of the TMS species is mainly the same as the IR fingerprint of the dimethypropylsilyl moieties of the tether. The slight increase only reflects an overall coverage of the surface occupied by both functions.

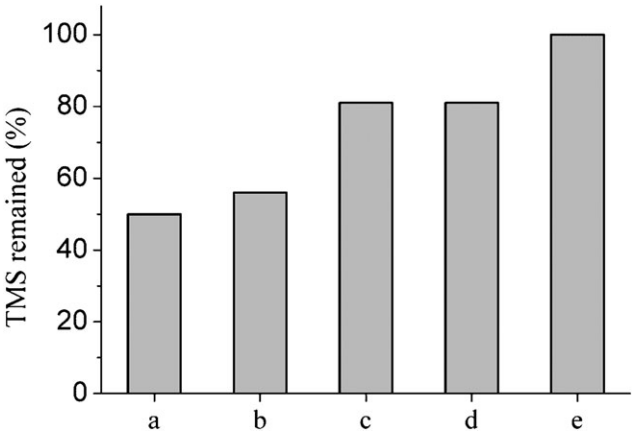

Fig. 10 Percentage of remaining surface TMS after 1h treatment of surfactant extraction (step **3** to **4** in Scheme 1) depending on repetition time, solvent, temperature and quantity of HCl: (a) 3 × (MeCN, 1 h, 60 °C, HCl 10 eq.), (b) 3 × (EtOH, 1 h, 40 °C, HCl 10 eq), (c) 1 × (EtOH, 1 h, 40 °C, HCl 10 eq), (d) 1 × (EtOH, 1 h, 40 °C, HCl 1.1 eq) and (e) 1 × (EtOH, 1 h, 0 °C, 1.1 eq).

Elemental analysis was here our only source for coverage estimation as reported in Table 3. The data reveal that TMS coverage that is calculated to be *ca.* 78% in material **5** is about the same as (77%) before the grafting and the derivatization of the tether. The overall coverage by both function reaches 96% consistently with the step (**4** → **5**) of Scheme 1.

However, the nature of the species produced is more problematic than the quantification at this step. Indeed, the strong reactivity of the isocyanate function with any nucleophile like H_2O, Si–OH, R–NH_2, may raise some questions on whether a unique species, or several different species, might be generated on the surface. The three most probable species that may exist on the surface are reported on Scheme 2: reactivity with water molecules (amine **7**), with surface silanol (carbamate **8**) and with neighbour grafted isocyanate after partial hydrolysis of the amino group (urea **9**). It is not easy to distinguish those species, in particular their ^{13}C CPMAS NMR fingerprints are relatively close one to each other. Nevertheless, one efficient means to detect the amine form **7** is to use benzaldehyde as molecular probe. The coupling reaction between –NH_2 and –CHO groups is instantaneous and complete at room temperature after 1 h in dichloromethane for their molecular analog (benzaldehyde and propylamine). The aromatic carbons of the benzaldehyde molecules serve as a specific signature on the NMR spectra at about 130 ppm. In our case, no aromatic signals were observed after the reaction between material **5** and one equivalent of benzaldehyde, which is consistent with no, or very few, species **7** on the surface. Considering now species **8** and **9**, there is no evidence of their presence on the surface. Indeed, the overall surface coverage obtained with TMS and tether species should limit the accessibility to silanol, and avoid the formation of **8**. Furthermore, the use of strict experimental conditions (fresh isocyanate, activated material **4** and distilled solvent) should have prevented any or most of the conversion of isocyanate moieties into amine and further coupling with a neighbouring isocyanate function, leading to **9**. However, if we consider a material covered only with TMS and expected urea **5**, we do not succeed in explaining the elemental analysis in a coherent way. So we introduce species **9** to the surface, and in correlation with TGA measurements, we estimate their proportion at about 3 : 1 for species **5** to **9**. Finally, the addition of about 15% of free aminomethylpyridine, apparently to the pores, leads to the use of material **5** in the sequence of the catalyst synthesis.

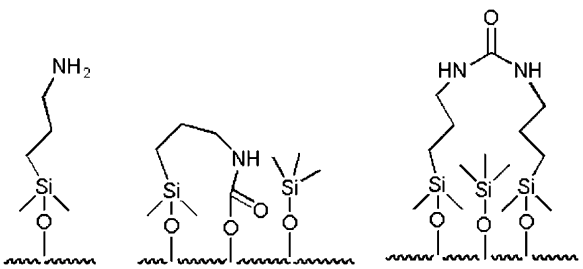

Scheme 2 Different tethers resulting from isocyanate surface reactions in material **5**: with water molecules (amine **7**), with surfacic silanol (carbamate **8**) and with neighbour grafted isocyanate (urea **9**).

The system after the fixation of the ruthenium (material **6**) gets even more complex, raising the question not only on the nature of ruthenium but also on the fate of the organic modification made in the previous steps. Surprisingly one of the questions that found a reasonable answer was the nature of the metal site.

According to the voltammograms and the dependence with the scan rate of the oxidative and reducing current can show that there is a unique type of site characterised by a very low electron diffusion rate, compatible with localisation inside the 2D channel of the LUS silica. The voltammograms are reversible showing that the ruthenium species at both oxidation states (II) and (III) keep or retrieve the same coordination. In addition, the oxidation potential of 500 mV and 550 mV *vs.* $AgNO_3$|Ag for material **6** and the complex [$Ru(dmp)_2PyCl$] (**[Ru2]**), respectively, are close to one another. A ligand substitution produces a very strong shift in the oxidation potential. For instance the $Ru(dmp)_2Cl_2$ exhibits in the same conditions an oxidation potential of −60 mV *vs.* $AgNO_3$|Ag. The slight difference of 50 mV accounts for a difference of environment of the complex in the pore of the material and in a bulk solution. Since the nature of the surface in such a type of silica is more likely the same in the exterior and as in the interior, there are also grafted complexes in the external part of the grains or fibers. However the external surface that accounts for to *ca.* 30 $m^2\ g^{-1}$, is 33 times smaller than the internal surface. One expects external grafted species at about the same ratio, *i.e.*, in a negligeable amount to affect the present data. Therefore, it is likely that the grafted complex is effectively the [$Ru(dmp)_2$(Py@LUS)Cl][Cl] as depicted on Scheme 1. In addition, material **6** shows reasonable catalytic activity (indeed slightly higher) than the homogeneous catalyst reacting in the same conditions with a selectivity comparable to that of the homogeneous complex [$Ru(dmp)_2PyCl$] toward sulfoxide. This also reinforces the assignment proposed here.

The origin of an absorption peak at relatively high wavelength, 700 nm, for material **6** originally raised a lot of questioning about the nature of the Ru coordination but

found no answer yet. Since both molecular analog, [Ru(dmp)$_2$PyCl], and material **5** (before fixation of the complex) do not exhibit this feature, one may invoke either the presence of the urea in the vicinity of the immobilised complex and/or the effect of the confinement in a nanopore with different electrostatic properties.

Finally, it is worth noticing that material **6** shows no deactivation during three runs and no metal leaching was detected. This is consistent with a relatively stable anchoring of the complex *via* the Ru–Py bond. This open opportunities for further studies of such complexes and their catalytic activities.

5. Conclusion

A multi step synthesis approach has been successfully applied to obtain the fixation of a Ru complex within the pore of a 2D hexagonal porous mesostructured silica. A quasi-molecular control has been applied as much as possible. First, the internal surface of the nano-channels were prepared according to a molecular patterning method consisting in partial coverage with trimethylsilyl groups in presence of surfactant molecules. Second, the surface deprotection is performed using a careful acidic extraction of the surfactant. Third, the isocyanatopropyldimethyl-chlorosilane is reacted with the surface silanol groups without apparent displacement of the grafted TMS groups. The so-obtained isocyanato tethers are readily derivatizated by reaction with 4-aminomethylpyridine leading to the fixation of the pyridinyl function *via* the formation of a urea. Fourth, the pyridinyl tether is involved in the substitution of one chloro ligand of the Ru(dmp)$_2$Cl$_2$ resulting in the covalent fixation of the complex described as [Ru(dmp)$_2$(Py@LUS)Cl][Cl]. The latter is found to be active in the catalytic oxidation of methylphenylsulfide into sulfoxide with high selectivity as its molecular precursor. At each step the intermediate materials were thoroughly characterised with a panel of techniques, including X-ray diffraction, elemental analysis, ^{29}Si and ^{13}C solid state NMR, diffuse reflectance UV-vis and FT-IR spectroscopies, and cyclic voltamperometry. Site isolation, unicity and localisation are achieved in the confined space of the nanopores of the silica matrix. The method developped here can be generalized to other inert complexes. For labile complexes the fixation by a polydentate ligand is more reasonable to avoid metal leaching during its utilisation in catalysis, for instance.

Acknowledgements

We thank the analytical services of the Institut des Recherches sur la Catalyse in Villeurbanne, especially Chantal Lorentz and Marie-Thérèse Gimenez. We thank also the Centre de Diffractométrie Henri Longchambon, especially Ruben Vera. Both CNRS and 'Région Rhône-Alpes' ('Thématique prioritaire' No. 301439201/E038131747/ENS2006) are acknowledged for their financial support.

References

1 (*a*) G. Sartori, R. Ballini, F. Bigi, G. Bosica, R. Maggi and P. Righi, *Chem. Rev.*, 2004, **104**(1), 199; (*b*) A. Corma and H. Garcia, *Chem. Rev.*, 2003, **103**(11), 4307.
2 (*a*) C. Li, H. Zhang, D. Jiang and Q. Yang, *Chem. Commun.*, 2007, 547; (*b*) C. Li, *Catal. Rev.—Science and Engineering*, 2004, **46**(3), 419.
3 B. C. Gates, in *Catalytic Chemistry*, Wiley, New York, 1992.
4 H. Yamaguchi, T. Hirano, H. Kiminami, D. Taura and A. Harada, *Org. Biomol. Chem.*, 2006, **4**, 3571.
5 (*a*) S. Coman, F. Cocu, V. I. Pârvulescu, B. Tesche, H. Bonneman, J. F. Roux, S. Kaliaguine and P. A. Jacobs, *J. Mol. Catal. A: General*, 1999, **146**, 247; (*b*) S. Coman, M. Florea, F. Cocu, V. I. Pârvulescu, P. A. Jacobs, C. Danumah and S. Kaliaguine, *Chem. Commun.*, 1999, 2175.
6 M. Florea, M. Sevinci, V. I. Pârvulescu, G. Lemay and S. Kaliaguine, *Microporous Mesoporous Mater.*, 2001, **44–45**, 483.
7 V. Ritleng, C. Sirlin and M. Pfeffer, *Chem. Rev.*, 2002, **102**, 1731.
8 T. Naota, H. Takaya and S. Murahashi, *Chem. Rev.*, 1998, **98**, 2599.
9 (*a*) G. A. Barf and R. A. Sheldon, *J. Mol. Catal. A: Chem.*, 1995, **102**, 23; (*b*) C. M. Che, K. W. Cheng, M. C. W. Chan, T. C. Lau and C. K. Mak, *J. Org. Chem.*, 2000, **65**, 7996.
10 (*a*) T. J. Meyer and M. H. V. Huynh, *Inorg. Chem.*, 2003, **42**, 8140; (*b*) L. S. Stultz, R. A. Binstead, M. S. Reynolds and T. J. Meyer, *J. Am. Chem. Soc.*, 1995, **117**, 250; (*c*) J. R. Bryant and J. M. Mayer, *J. Am. Chem. Soc.*, 2003, **125**, 10351; (*d*) A. S. Goldstein, R. H. Beer and R. S. Drago, *J. Am. Chem. Soc.*, 1994, **116**, 2424; (*e*) A. S. Goldstein and R. S. Drago, *J. Chem. Soc., Chem. Commun.*, 1991, **21**.
11 M. Chavarot, S. Ménage, O. Hamelin, F. Chanay, J. Pécault and M. Fontecave, *Inorg. Chem.*, 2003, **42**, 4810.
12 D. Trong On, D. Desplantier-Giscard, C. Danumah and S. Kaliaguine, *Appl. Catal., A*, 2003, **253**, 545.
13 A. Corma, *Chem. Rev.*, 1997, **97**, 2373.
14 C. T. Kresge, M. E. Leonowicz, W. J. Roth, J. C. Vartuli and J. S. Beck, *Nature*, 1992, **359**, 710.
15 J. S. Beck, C. T. Wu Chu, I. D. Johnson, C. T. Kresge, M. E. Leonowicz, W. J. Roth and J. C. Vartuli, WO 91/11390, 1991.
16 (*a*) K. Wilson, A. F. Lee, D. J. Macquarrrie and J. H. Clark, *Appl. Catal. A: Gen.*, 2002, **228**(1–2), 127; (*b*) C. Yoshina Ishii, T. Asefa, N. Coombs, M. J. Maclachlan and G. A. Ozin, *Chem. Commun.*, **999**, 2539; (*c*) S. Inagaki, S. Guan, Y. Fukushima, T. Ohsuna and O. Terasaki, *J. Chem. Soc.*, 1999, **121**, 9611; (*d*) T. Asefa, M. J. Maclachlan, N. Coombs and G. A. Ozin, *Nature*, 1999, **402**, 867.
17 M. A. Wahab and C. S. Ha, *J. Mater. Chem.*, 2005, **15**(4), 508.
18 V. Dufaud and J. M. Basset, *Angew. Chem., Int. Ed.*, 1998, **37**(6), 806.
19 M. Alvaro, A. Corma, D. Das, V. Fornés and H. Garcia, *J. Catal.*, 2005, **231**, 48.
20 (*a*) D. J. Macquarrie, D. Brunel, G. Renard and A. C. Bland, *Stud. Surf. Sci. Catal.*, 2001, **135**, 312; (*b*) T. Martin, A. Galarneau, D. Brunel, J. Izard, V. Hulea, A. C. Blanc, S. Abramson, F. Di Renzo and F. Fajula, *Stud. Surf. Sci. Catal.*, 2001, **135**, 178; (*c*) D. Brunel, A. Cauvel, F. Fajula and F. Di Renzo, *Stud. Surf. Sci. Catal.*, 1995, **97**, 173.
21 J. L. Zhang, Y. L. Liu and C. M. Che, *Chem. Commun.*, 2002, 2906.
22 B. De Clercq, F. Lefebvre and F. Verpoort, *Appl. Catal. A: Gen.*, 2003, **247**, 345.
23 T. Joseph, S. S. Deshpande, S. B. Halligudi, A. Vinu, S. Ernst and M. Hartmann, *J. Mol. Catal. A: Chem.*, 2003, **206**, 13.
24 Robert J. P. Corriu, F. Embert, Y. Guari Dr. **1**, C. Reyé and Roger Guilard, *Chem.–Eur. J.*, 2002, **8**, 5732.
25 (*a*) M. Stempniewicz, M. Rohwerder and F. Marlow, *Chem. Phys Chem.*, 2007, **8**, 188; (*b*) V. Hulea, M. Lalleman, A. Finiels and F. Fajula, *Stud. Surf. Sci. Catal.*, 2005, **158**, 1621.
26 (*a*) H. Q. Yang, L. W. G. Su, Q. H. Yang and L. Can, *J. Catal.*, 2007, **248**, 204; (*b*) A. Corma and H. García, *Eur. J. Inorg. Chem.*, 2004, **6**, 1143; (*c*) P. P. Knops-Gerrits, D. D. Vos, F. T. Thibault-Starzyk and P. A. Jacobs, *Nature*, 1994, **369**, 543; (*d*) D. E. Devos, J. L. Meinershagen and T. Bein, *Angew. Chem., Int. Ed.*, 1996, 35.

27 L. Bonneviot, M. Morin and A. Badiei, Patent WO 01/55031 A1, 2001.
28 (*a*) L. Bonneviot, A. Badiei and N. Crowther, Patent WO 0216267, 2002; (*b*) A. Badiei and L. Bonneviot, *Inorg. Chem.*, 1998, **37**, 4142; (*c*) A. Badiei, L. Bonneviot, N. Crowther and G. M. Ziarani, *J. Organomet. Chem.*, 2006, **691**(26), 5911.
29 K. S. W. Sing, D. H. Everett, R. A. W. Haul, L. Moscow, R. A. Pierotti, T. Rouquerol and T. Siemienewska, *Pure Appl. Chem.*, 1985, **57**, 603.
30 J. S. Beck, J. C. Vartuli, W. J. Roth, M. E. Leonowicz, C. T. Kresge, K. D. Schmitt, C. T. W. Chu, D. H. Olson, E. W. Sheppard, S. B. McCullen, J. B. Higgins and J. L. Schlenker, *J. Am. Chem. Soc.*, 1992, **114**(27), 10834.
31 S. Abry, B. Albela and L. Bonneviot, *C.R. Chimie*, 2005, **8**, 741.
32 G. Engelhardt and D. Michel, in *High-Resolution Solid-State NMR of silicates and Zeolithes*, Wiley, New York, 1987.
33 M. Benitez, D. Das, R. Ferreira, U. Pischel and H. Garcia, *Chem. Mater.*, 2006, **18**(23), 5597.
34 A. Juris, V. Balzani, F. Barigelletti, S. Campagna, P. Belser and A. von Zelewsky, *Coord. Chem. Rev.*, 1988, **84**, 85.
35 E. Laviron, *J. Electroanal. Chem.*, 1980, **112**, 1.
36 C. P. Andrieux and J. M. Savéant, *J. Electroanal. Chem.*, 1980, **111**, 377.
37 E. Martinez-Fernandez, D. Grosso, C. Boissière, C. Sanchez, O. Oms, D. Leclercq, A. Vioux, F. Miomandre and P. Audebert, *J. Mater. Chem.*, 2006, **16**, 3762.